UDK 634.616:549.691
Original scientific article/Izvirni znanstveni članek

ISSN 1580-2949
Mater. Tehnol.

# AMORPHOUS SILICA-SUPPORTED $ZrO_2$-$WO_3$ MESOPOROUS NANOCOMPOSITE FROM AGRO-INDUSTRIAL WASTE (COCONUT COIR): SUSTAINABLE HETEROGENEOUS CATALYST FOR 4H-CHROMENE SYNTHESIS

# AMORFNA SILIKA PODPRTA Z $ZrO_2$-$WO_3$ MEZOPOROZNIM NANOKOMPOZITOM IZ AGRARNIH INDUSTRIJSKIH ODPADKOV (KOKOSOVA VLAKNA ZUNANJE LUPINE) KOT HETEROGENI KATALIZATOR ZA TRAJNOSTNO SINTEZO 4H-KROMENA

**Stanelybritto Maria Arul Francis[1], Sharmil Suganya Rajan Babu[2#], Vaithianathan Rasappan[1#], Venugopal Thiruvengadam[1*]**

[1]Department of Chemistry, Government College of Engineering, Salem 636011, Tamil Nadu, India
[2]Department of Electrical and Electronics Engineering, Government College of Engineering, Salem 636011, Tamil Nadu, India
[#]These authors contributed equally (co-second authors).

*Prejem rokopisa – received: 2025-04-17; sprejem za objavo – accepted for publication: 2025-12-04*

doi:10.17222/mit.2025.1437

This study presents a green and cost-effective preparation of amorphous silica-supported $ZrO_2$-$WO_3$ mesoporous nanocomposite from agro-industrial waste, specifically coconut coir. Amorphous silica (AS) was obtained through a sustainable extraction process from coconut coir, and the amorphous silica-supported-$ZrO_2$-$WO_3$ (ASS-ZWOM) nanocomposite was prepared using the wet impregnation technique. The structural features and compositional details of the prepared ASS-ZWOM nanocomposite were evaluated using several advanced analytical techniques. FT-IR analysis confirmed the Si-O-Si vibrations, and the composite exhibited additional Zr-O and W-O bands, indicating the successful metal oxide incorporation. FE-SEM images revealed that the nanocomposites are below 100 nm. Energy-dispersive X-ray spectroscopy was used for element composition, and Raman spectroscopy for studying molecular vibrations. BET measurement demonstrated mesoporosity with a surface area of 2.68 $m^2/g$ and a pore diameter of 2.36 nm. This study highlights the potential of agro-industrial waste-derived materials for producing high-performance catalysts, demonstrating a sustainable catalytic route for synthesizing 4H-chromene.

Keywords: coconut coir, silica, mesoporous, nanocomposite, heterogeneous catalyst, multicomponent reaction

V članku avtorji predstavljajo študijo okolju prijazne in cenovno učinkovite priprave amorfne silike podprte z $ZrO_2$-$WO_3$ mezoporoznim nanokompozitom iz agrarnega industrijskega odpadka (kokosovih vlaken zunanje lupine). Amorfno siliko (AS) so avtorji pridobili s pomočjo ekstrakcijskega procesa iz kokosovih vlaken. Amorfno siliko so nato s postopkom mokre impregnacije obdelali z $ZrO_2$-$WO_3$ (ASS-ZWOM) nanokompozitom. Tako izdelane ASS-ZWOM nanokompozite so detajlno analizirali. Za določitev strukturnih lastnosti in sestave so uporabili različne napredne analitske tehnike. FT-IR analiza je potrdila vibracije Si-O-Si. Uspešno vključitev kovinskih oksidov je potrdila analiza kemijske sestave z ugotovljenimi dodatnimi pasovi Zr-O in W-O. Slike izdelne s pomočjo vrstičnega elektronskega mikroskopa na emisijo polja (FE-SEM) so pokazale, da je velikost delcev nanokompozita pod 100 nm. Spektroskopijo na osnovi disperzije rentgenskih žarkov (EDXS; angl.: Energy-dispersive X-ray spectroscopy) so avtorji uporabili za določitev elementne kemijske sestave in Ramanovo spektroskopija za študiranje molekularnih vibracij. S pomočjo meritev na osnovi BET metode so določili mezoporoznost kompozita; specifično površino preseka 2,68 $m^2/g$ in premer por 2,36 nm. S to študijo so avtorji osvetlili potencial materialov iz agro-industrijskih odpadkov za sintezo 4H-kromena in proizvodnjo drugih visoko zmogljivih katalizatorjev preko okolju prijazne in cenovno ugodne poti.

Ključne besede: kokosova vlakna iz zunanje lupine, silika, mezoporoznost, nanokompozit, heterogeni katalizator, večkomponentna reakcija

## 1 INTRODUCTION

The coir processing industry produces a considerable amount of coir waste, a lignocellulosic byproduct that presents notable challenges for disposal. However, recycling and repurposing this waste offer potential environmental and economic advantages.[1] Consequently, recycling agro-industrial waste is recognised as a potential strategy to mitigate environmental degradation and public health risks.[2] Metal oxides, such as alumina, silica, and aluminosilicates, serve as primary supports in heterogeneous catalysts. Among the various solid supports, mesoporous silica has emerged as an effective catalyst support owing to its exceptional thermal stability, extensive surface area, and adjustable pore dimensions.[3] However, the conventional preparation of mesoporous silica involves expensive and environmentally detrimental precursors like tetraethylorthosilicate, sodium silicate, and silicic alkoxides.[4] This challenge has prompted researchers to explore alternative sources of silica from agro-in-

*Corresponding author's e-mail:
venugopalt@gcesalem.edu.in (Venugopal Thiruvengadam)

dustrial wastes, offering a greener and more cost-effective solution.

Sustainable methods for producing mesoporous silica from agro-industrial waste have been explored in response to these challenges. Silica-containing agricultural crop wastes from sugarcane, rice, wheat, corn, and bamboo can be used to generate materials with $SiO_2$ percentages of (88, 98, 86, 60 and 74) %, respectively.[5] Coconut coir has been identified as an alternative source for the preparation of amorphous silica because it is highly available and prevents solid waste generation.[6] Despite this, coconut coir waste from mat industries is often incinerated as domestic fuel. Tungsten oxide-based materials, first identified by Hino and Arata as strongly acidic, have garnered attention as a promising class of solid acids.[7] The research demonstrated that $WO_x/ZrO_2$ catalysts exhibited high catalytic activity for the isomerization of alkanes, with excellent cracking selectivity at low temperatures. This performance depends on factors such as dispersion and surface density of WOx species, their oxidation state, reaction temperature, and surface area of $ZrO_2$.[8] Furthermore, $WO_x/ZrO_2$ catalysts display superior thermal and chemical stabilities, making them attractive for various industrial applications.[9] Although considerable progress has been achieved in the development of $WO_3/ZrO_2$-based catalysts, further investigation is still needed to fully understand their catalytic behaviour and optimise their performance for broader applications. Building on the research, our study investigates the catalytic performance of coconut coir-derived amorphous silica supported with $WO_3/ZrO_2$, applying it to the synthesis of 4H-chromene. The 4H-chromene compounds are crucial in drug development because of their diverse pharmacological and biological activities, including diuretic, antioxidant, antifungal, and antiviral properties, as well as anticancer activity.[10,11] Additionally, these groups of compounds are used in agrochemicals, cosmetics[12] and laser dyes.[13]

In light of the need for both sustainable material sourcing and improved catalytic efficiency, this work focuses on converting coconut coir into amorphous silica using cost-effective and environmentally friendly methods. The resulting amorphous silica will be applied in the preparation of ASS-ZWOM nanocomposite. Based on existing reports, this work represents the first instance where ASS-ZWOM has been applied as a solid heterogeneous catalyst in a multicomponent reaction for the synthesis of 4H-chromenes. This approach aims to foster the development of environmentally sustainable catalytic systems that hold considerable relevance in industrial applications.

## 2 EXPERIMENTAL PART

### *2.1 List of chemicals and materials*

Zirconium chloride octahydrate, ammonium metatungstate, hydrochloric acid, nitric acid, ethyl acetate, methanol, toluene, chloroform, acetonitrile, hexane, and ethanol were sourced from Loba Chemie Pvt. Ltd, India. Dried coconut coir was sourced from a local Tiruchirappalli, Tamil Nadu mat-making company. Nitrobenzaldehyde, dimedone, malononitrile, and Silica gel 60 $F_{254}$ TLC plates were all obtained from Merck Chemicals Private Limited.

### *2.2 Extraction of amorphous silica (AS)*

Amorphous silica was extracted using an acid treatment followed by a high-temperature calcination-modified method based on Balamurugan et al.[14] Initially, 100 g of dried coconut coir waste were placed in a beaker, and 500 mL of 0.1 N hydrochloric acid (HCl) solution was added. The whole mixture was allowed to sit undisturbed at room temperature for 24 h. Following this, the solution was decanted, and the coir was thoroughly washed with distilled water (DW) until the pH of the filtrate reached 7.

The coir was first thoroughly washed and then dried in a hot air oven at 100 °C for six hours to remove any residual moisture. Afterwards, the dried coir was placed in a silica crucible and heated in a furnace at 700 °C for three hours under an inert atmosphere. The obtained residue (1 g) was combined with a 100 mL solution of 3 % hydrochloric acid (HCl) in a round-bottomed flask and subjected to reflux for three hours. Following the reflux process, the mixture was filtered, and the solid residue was rinsed with distilled water (DW) until the pH of the filtrate reached neutrality (7). The white precipitate was then dried in a hot oven at 100 °C for three hours. Subsequently, the dried silica was treated with 5 M nitric acid for four hours and washed with DW. Finally, it was transferred to a silica crucible and calcinated at 700 °C for three hours in a furnace.

### *2.3 Preparation of the ASS-ZWOM nanocomposite*

The ASS-ZWOM nanocomposite was prepared using amorphous silica (AS) derived from coconut coir waste, with modification to the procedure reported by Shanmugam Manimaran et al.[15] Initially, 10 g of AS and 2 g of zirconium chloride octahydrate were dissolved in 100 mL of DW and stirred continuously at 80 °C for eight hours. After complete evaporation of water, the resulting residue was collected, transferred into a silica crucible, and calcinated at 550 °C in the furnace for about three hours. In the next step, 2 g of the prepared silica-$ZrO_2$ composite were mixed with 0.2 g of the ammonium metatungstate and 100 mL of DW. The mixture was stirred at 100 °C for three hours, followed by evaporation of water. The remaining solid residue was subjected to calcination at 850 °C for about three hours, yielding the final ASS-ZWOM nanocomposite.

### *2.4 Procedure for catalytic activity evaluation*

A mixture containing 0.3 (mg) of ASS-ZWOM nanocomposite, 1 mmol of 4-nitrobenzaldehyde (1), 1 mmol of malononitrile (2), and dimedone (3) was heated at 80 °C under solvent-free conditions with continuous magnetic stirring in a round-bottom flask (RB). The progress of the reaction was monitored by thin-layer chromatography (TLC) using a solvent system comprising ethyl acetate and hexane in a 3:4 ratio. Once the reaction was complete, 10 mL of hot ethanol was introduced into the RB to facilitate the separation of the catalyst. The mixture was filtered, and the filtrate was concentrated under reduced pressure. The resulting product was then purified through recrystallization using ethanol.

White solid, m.p. 175–178 °C. Product 4: $^1$H NMR (400 MHz, DMSO-$d_6$) $\delta$ 8.18 (d, J = 8.4 Hz, 2H, aromatic-H), 7.45 (d, J = 8.3 Hz, 2H, aromatic-H), 7.17 (s, 2H, $NH_2$), 4.37 (s, 1H, C-H), 2.55 (s, 2H, $CH_2$), 2.27 (d, J = 16.1 Hz, 1H, $CH_2$), 2.12 (d, J = 16.1 Hz, 1H, $CH_2$), 1.05 (s, 3H, $CH_3$), 0.97 (s, 3H, $CH_3$).

## 3 Characterisation

The surface functional groups of the material were examined through Fourier-transform infrared spectroscopy using the KBr pellet technique on the IR Affinity-1 system (Shimadzu, Japan) at the Indian Institute of Technology (IIT), Jammu. The crystalline phases were identified through powder X-ray diffraction using a Rigaku Dmax-RC instrument equipped with Ni-filtered Cu K$\alpha$ radiation ($\lambda$ = 0.154059 nm) at IIT Jammu. Textural and morphological features were observed with a JSM-7900F field-emission scanning electron microscope (FE-SEM) at the SAPTARSHI facility of IIT Jammu. Elemental composition was assessed by energy-dispersive X-ray spectroscopy using a SIGMA HV – Carl Zeiss system with a Bruker Quantax 200 – Z10 detector. Raman spectra were obtained with a RENISHAW basic series spectrometer (514 LASERS) at the Sophisticated Analytical Instrumentation centre, Tezpur University. The nitrogen adsorption-desorption measurement for determining the surface area and pore size characteristics was performed using a Quantachrome BET analyser at the Material Analysis and Research Centre, Bengaluru. Proton NMR ($^1$H NMR) spectra were collected on a Bruker Advance III spectrometer at the Vellore Institute of Technology, India.

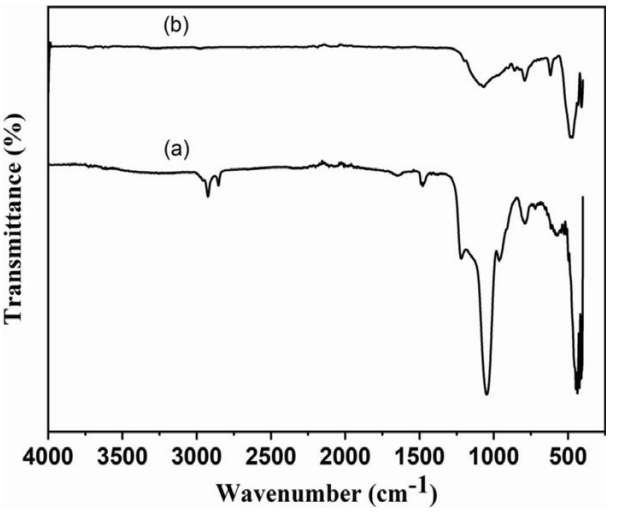


**Figure 1:** FT-IR spectra: a) amorphous silica, b) ASS-ZWOM nanocomposite

## 4 RESULTS AND DISCUSSION

### *4.1 IR spectroscopy*

The functional groups and vibrational modes present in the nanocomposite were examined using Fourier transform infrared spectroscopy (FT-IR). Spectra 1a and 1b illustrate the transmittance intensities of the AS and ASS-ZWOM nanocomposite, specifically focusing on the transmittance peaks observed within a wavenumber range of 0–4000 cm$^{-1}$.

Spectrum 1a shows a peak at ≈1050 cm$^{-1}$ attributed to the Si-O-Si stretching vibrations.[16] Moreover, a significant peak at ≈448 cm$^{-1}$ is observed, representing the out-of-plane bending vibrations of Si-O bonds. Further, peaks were detected at ≈790 cm$^{-1}$, representing the bending vibration of Si-O.[17] Notably, there is no transmittance peak in the region of 4000–3400 cm$^{-1}$, due to the lack of hydroxyl (OH) groups and $Si(OH)_4$ formation in the prepared silica.[18]

Spectrum 1b highlights different absorption bands that correspond to metallic interactions, such as metal-oxygen-metal (M–O–M), oxygen-metal-oxygen (O–M–O), and metal-hydroxyl (M–OH) linkages, within the range of 1200–410 cm$^{-1}$ (M = Zr, Si).[19] A broad peak at ≈1093 cm$^{-1}$ was observed, attributed to overlapping stretching vibrations of the Si-O-Si linkage and the Si-O-Zr bonds.[20] Another prominent peak at ≈862 cm$^{-1}$ is associated with tungsten-oxygen (W-O) bonds in tungsten oxide, making a characteristic feature of the nanocomposite.[21] The peaks at ≈940 cm$^{-1}$, ≈890 cm$^{-1}$, and ≈860 cmm$^{-1}$ are linked to different vibrational modes of tungsten bonds, including terminal oxygen (W = O), angularly shared oxygen connections (W-O-W), and edge-sharing octahedron connections (W-O-W), respectively.[22] The peak appearing near ≈796 cm$^{-1}$ reflects the vibrational contribution of the W-O-W bond,[23] while the peak observed at ≈474 cm$^{-1}$ arises from Si–O and Zr–O related bonds.[24] Additionally, the low-intensity band at ≈ 659 cm$^{-1}$ confirms the presence of Zr–O bonds within the composite structure.[25] In amorphous silica, the Si–O bond typically appears as a peak at ≈1045 cm$^{-1}$. In contrast, the Si–O bond peak is shifted at ≈1087 cm$^{-1}$ in the ASS-ZWOM nanocomposite, due to the incorporation of $ZrO_2$ and $WO_3$ into the silica matrix. This spectral analysis demonstrates the successful integration of metallic

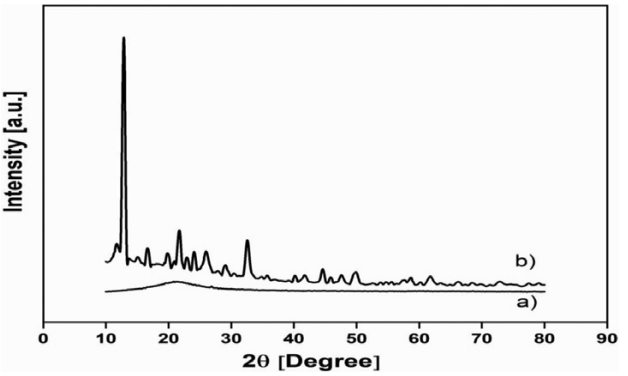


**Figure 2:** a) XRD spectrum of amorphous silica, b) XRD spectrum of ASS-ZWOM nanocomposite

oxides ($ZrO_2$ and $WO_3$) into the silica framework and provides valuable insights into the bond interactions of the ASS-ZWOM nanocomposite.

### *4.2 XRD analysis*

X-ray diffraction (XRD) analysis was performed to identify the crystalline phases, assess the structural purity, and estimate the crystalline size of the AS produced from the coconut coir, as shown with Spectra 2a and 2b. The XRD pattern of AS displays a broad hump at $2\theta \approx 21.8°$, corresponding to the (111) reflection, which aligns well with the observation previously documented by Maseko et al.[26] The observed pattern closely aligns with the standard diffraction data from JCPDS card No. 00-045-0131.[27] The formation of AS is strongly influenced by parameters such as the calcination temperature, time, and the overall stability of the biomass during the process. Especially, the presence of an amorphous silica phase is linked to calcination temperatures ranging between 500–800 °C, as described by Arnaldo et al.[28] Amorphous silica is considered non-toxic and does not pose a risk of silicosis when in contact with biological systems.[29] The average crystalline size of the AS was determined by the Scherrer equation as $D = K\lambda / (\beta\cos\theta)$. In this formula, $D$ is the crystalline size, $K$ (0.89) represents the Scherrer constant, $\lambda$ (0.15406 nm) is the wavelength of X-ray radiation (CuK$\alpha$), $\theta$ is the Bragg angle, and $\beta$ is the full width at half maximum (FWHM) of the diffraction peak in radians. Using the Scherrer equation, the crystalline size of AS was estimated to be around 2 nm.

The X-ray diffraction (XRD) spectrum of the ASS-ZWOM nanocomposite is shown in Spectrum 2b, revealing detailed crystallographic information about the

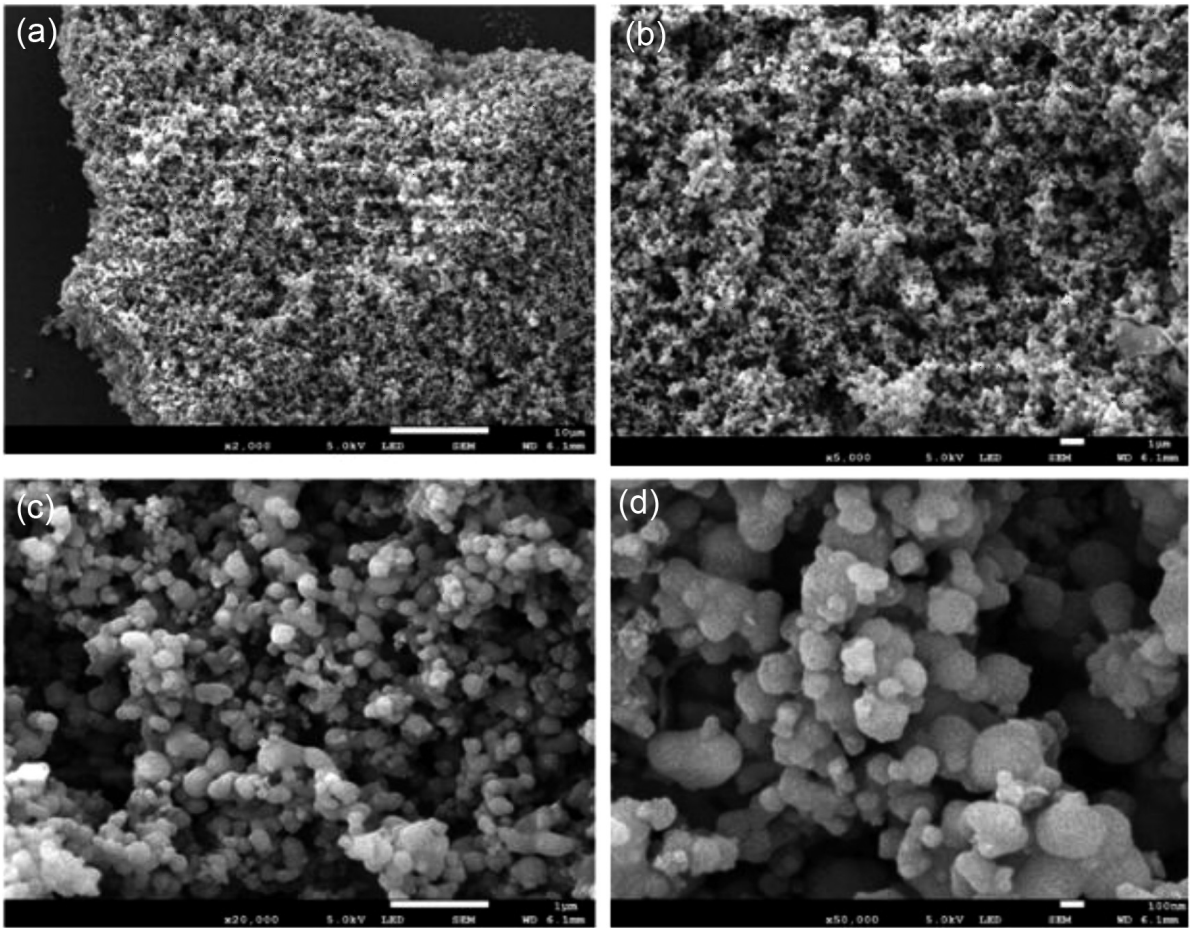


**Figure 3:** FE-SEM images of amorphous silica

material. The XRD analysis indicates the presence of cubic-phase tungsten oxide ($WO_3$) with distinct peaks observed at ≈23.62°, ≈33.67°, ≈41.47°, ≈48.43°, ≈54.56°, ≈60.24°, ≈70.74°, ≈75.74° and ≈78.04°. These peaks correspond to Miller indices (200), (220), (222), (400), (420), (422), (600), and (611), matching the standard reference pattern detailed in JCPDS card no. 00-046-1096.[30] Additionally, the XRD spectrum shows the $2\theta$ positions at ≈21.10°, ≈28.17°, ≈31.45°, ≈34.40°, ≈38.50°, ≈44.82°, ≈50.56°, ≈57.10°, ≈61.94°, ≈69.63°, ≈72.50°, and ≈76.98°, which are in good agreement with the standard pattern from JCPDS card no. 01-083-0944. These peaks correspond to Miller indices (011), (-111), (111), (020), (021), (112), (-122), (130), (130), (-213), (123), (041), and (-141), confirming the formation of the monoclinic zirconia (ZrO2) crystal structure.[31] The analysis indicates that the average crystalline size of the ASS-ZWOM nanocomposite, estimated using the Scherrer equation, is about 13 nm. In conclusion, the XRD analysis of the ASS-ZWOM nanocomposite demonstrates the successful formation of cubic-phase $WO_3$ and monoclinic $ZrO_2$, both of which contribute to the structural characteristics. The catalyst with a similar $WO_3$/$ZrO_2$ particle size (≈10–15 nm) was reported to exhibit a strong catalytic activity, supporting the performance observed in this study.[32,33]

### *4.3 FE-SEM analysis*

Field emission scanning microscopy (FE-SEM) images of the AS and ASS-ZWOM nanocomposites were obtained at varying voltages (KV) and resolutions, providing detailed insights into their structural properties. **Figures 3** and **4** illustrate the AS and ASS-ZWOM nanocomposites at magnifications of 2000×, 10,000×, 25,000×, and 25,000×, respectively. The morphological analysis of AS is depicted in **Figures 3a** to **3d**, which reveal the presence of spherical particles exhibiting a porous structure. The observed agglomeration of silica particles can be attributed to the intrinsic characteristic of the biomass source derived from the coconut coir. The conditions employed during preparation, including temperature, time, and other preparation parameters, significantly influenced the hierarchical agglomeration and formation of the amorphous silica, ultimately contributing to its uniform morphology.[34] These images indicate that the minimum size of the AS is less than 100 nm.

The morphological analysis of the ASS-ZWOM nanocomposite, as shown in **Figures 4a** to **4d**, reveals a heterogeneous structure comprising spherical porous particles and plate-like formations, with the nanocomposite below 100 nm in size. Diverse structural arrangements indicate a complex morphology, which is characteristic of a composite material. The presence of the complex morphology suggests an interaction between

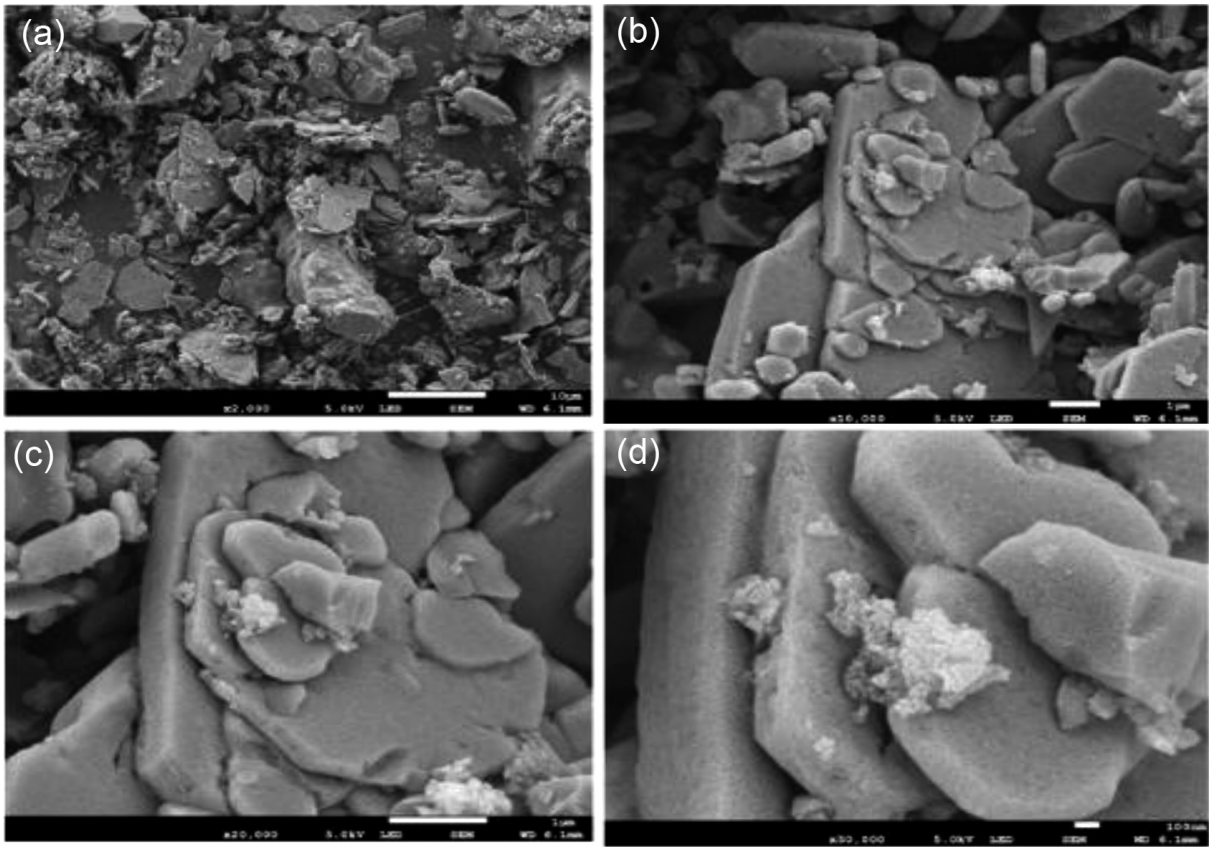


**Figure 4:** FE-SEM images of the ASS-ZWOM nanocomposite

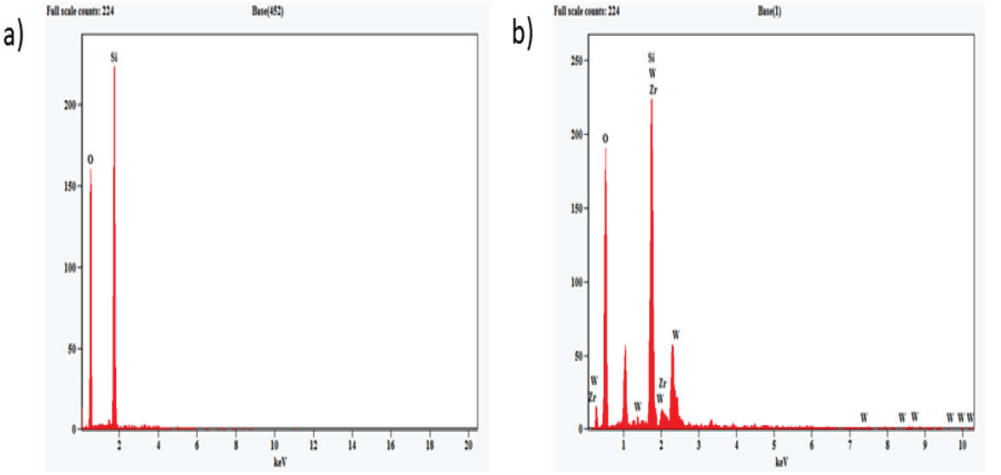


**Figure 5:** EDX spectra: a) amorphous silica, b) ASS-ZWOM nanocomposite

the AS and components of the nanoparticles during the preparation process. Although the ASS-ZWOM nanocomposite contains metal oxides ($ZrO_2$ and $WO_3$), the overall particle size remains in the nanometre range because it is dispersed within the silica matrix, which helps preserve the nanoscale morphology.

### *4.4 EDS analysis*

Energy-dispersive X-ray spectroscopy (EDS) was employed to examine the compositions of the AS and ASS-ZWOM nanocomposite, as presented in **Figures 5a** and **5b**. The EDS spectrum of AS, depicted in **Figure 5a**, reveals sharp and well-defined peaks corresponding to the elements of oxygen (O) and silica (Si), confirming the predominant silica in the sample.

In contrast, the EDS spectrum of the ASS-ZWOM nanocomposite, shown in **Figure 5b**, highlights the presence of silicon (Si), zirconium (Zr), oxygen (O), and tungsten (W), confirming that elements are successfully incorporated into the silica framework. Such consistent dispersion is crucial for improving the catalytic performance and stability of the nanocomposite. The EDS analysis thus confirms the compositional integrity of both the AS and ASS-ZWOM nanocomposite, with the latter exhibiting a multi-elemental composition due to the integration of zirconium and tungsten into the silica in the form of oxide.

### *4.5 Raman spectroscopy*

**Figures 6a** and **6b** illustrate the Raman spectra of the AS and ASS-ZWOM nanocomposite. The ASS-ZWOM nanocomposite displays well-defined and prominent peaks, contrasting amorphous silica (**Figure 6a**), which is less Raman active, exhibiting relatively smaller peaks. The Ramnan spectrum of AS shows only weak, broad features because of amorphous silica long-range structural order. The disordered Si-O-Si framework causes vibrational modes to broaden, leading to low-intensity humps rather than distinct Raman peaks.[35] Raman spectrum 6b, relating to the ASS-ZWOM nanocomposite, shows distinct peaks at (810, 718, 330 and 277) $cm^{-1}$, confirming the presence of $WO_3$. The bands observed at 810 $cm^{-1}$ and 718 $cm^{-1}$ arise from vibrational modes liked to W-O-W bridging stretches, whereas the band appearing at around 277 $cm^{-1}$ originates from bending vibrations. A weak band at 330 cm-1 corresponds to the bending vibration of O-W-O bonds within surface WOx species. Additionally, a low-intensity peak at 600 $cm^{-1}$ signifies the formation of the $ZrO_2$ phase in the nanocomposite.[36]

### *4.6 BET analysis*

The nitrogen adsorption/desorption isotherms of the ASS-ZWOM nanocomposite are illustrated in **Figure 7**, aligning with the type IV isotherms pattern and an H4 hysteresis loop, characteristic of mesoporous materials as per the IUPAC classification.[37] The BET analysis showed that the ASS-ZWOM nanocomposite features a surface area of 2.68 $m^2/g$, which represents the total surface area available per unit area. Additionally, the nano-

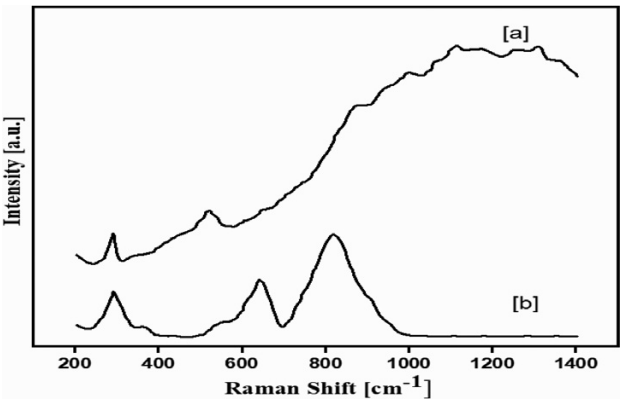


**Figure 6:** Raman spectra: a) amorphous silica, b) ASS-ZWOM nanocomposite

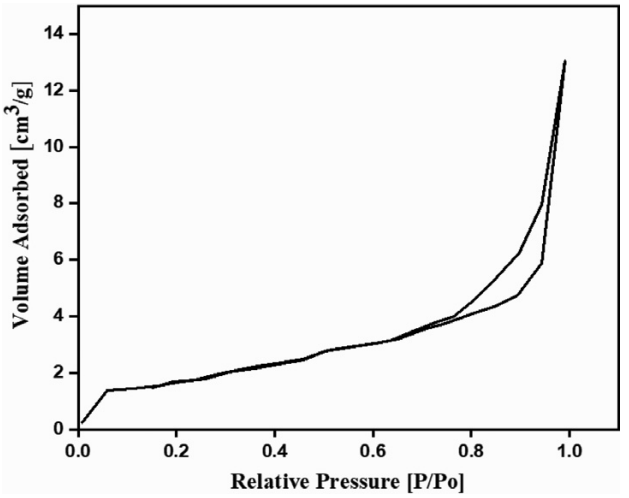


**Figure 7:** Nitrogen adsorption/desorption isotherms of the ASS-ZWOM nanocomposite

composite features a pore diameter of 2.36 nm and a pore volume of 0.002 $cc^3/g$, reflecting the overall volume of pores per unit mass. These structural features, including the moderate surface area and small pore size, enhance the catalytic performance of the ASS-ZWOM nanocomposite by providing a sufficient site for adsorption and facilitating the diffusion of reactants and products during catalytic reactions. The mesoporous nature of the composite is crucial for application as a nano-heterogeneous catalyst, allowing for improved reaction kinetics and mass transfer.

### *4.7 Catalytic activity of the ASS-ZWOM nanocomposite*

The catalytic efficiency of the ASS-ZWOM nanocomposite was evaluated using a three-component reaction involving dimedone, 4-nitrobenzaldehyde, and malononitrile (as shown in **Scheme 1**). This reaction served as a model reaction to assess the catalytic efficiency of the nanocomposite and to optimize the reaction conditions.

Herein, the synthesis of a product (4) was optimized by varying parameters such as amount of catalyst, solvent type, solvent-free (SF) conditions, and temperature, resulting in different product yields (**Table 1**). The control experiment was conducted in the absence of the catalyst with a negligible product formation. The influence of solvent and temperature (room temperature (RT), Reflux) was assessed by performing the reaction using 0.1 mg of the catalyst. The product yield was significantly lower, ranging from 9 % to 35 % (Entries 1–12). In contrast, under SF conditions, the product yield reached 83 % within 15 min at 80 °C (Entry 13). This result emphasized the superior efficiency of the catalyst in a solvent-free condition. To further optimize the reaction, different amounts of catalyst were tested under SF conditions at 80 °C, namely (0.2, 0.3, 0.4, and 0.5) mg. For entries 14–17, the product yields and times for different amounts of catalyst were 85 % (10 min), 89 % (10 min), 89 % (10 min), and 87 % (10 min), respectively.

**Table 1:** Synthesis of Product 4 catalysed using ASS-ZWOM nanocomposite under various conditions

| Entry | Amount of catalyst (mg) | Reaction medium | Temperature (°C) | Duration (min) | Product yield (%) |
|---|---|---|---|---|---|
| 1 | 0.1 | Ethanol | RT | 340 | 15 |
| 2 | 0.1 | Methanol | RT | 347 | 17 |
| 3 | 0.1 | Toluene | RT | 427 | 12 |
| 4 | 0.1 | Ethyl acetate | RT | 486 | 14 |
| 5 | 0.1 | Acetonitrile | RT | 327 | 11 |
| 6 | 0.1 | Chloroform | RT | 457 | 9 |
| 7 | 0.1 | Ethanol | Reflux | 130 | 35 |
| 8 | 0.1 | Methanol | Reflux | 210 | 33 |
| 9 | 0.1 | Toluene | Reflux | 350 | 24 |
| 10 | 0.1 | Ethyl acetate | Reflux | 309 | 27 |
| 11 | 0.1 | Acetonitrile | Reflux | 250 | 21 |
| 12 | 0.1 | Chloroform | Reflux | 350 | 18 |
| 13 | 0.1 | SF | 80 | 15 | 83 |
| 14 | 0.2 | SF | 80 | 10 | 85 |
| 15 | 0.3 | SF | 80 | 10 | 89 |
| 16 | 0.4 | SF | 80 | 10 | 89 |
| 17 | 0.5 | SF | 80 | 10 | 87 |
| 18 | No catalyst | Ethanol | Reflux | 90 | trace |

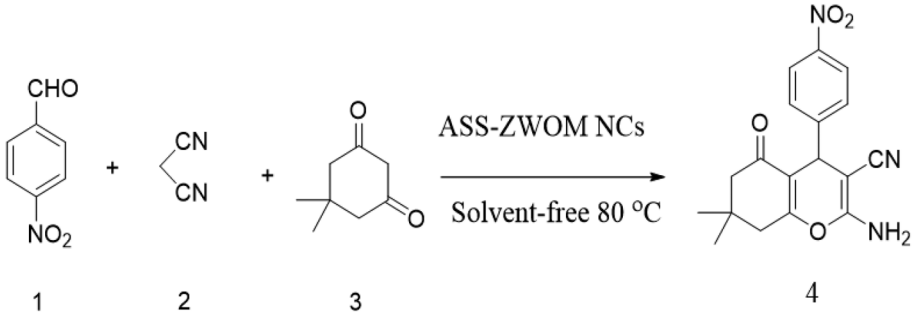


**Scheme 1:** Synthesis of 2-amino-7,7-dimethyl-4-(4-nitrophenyl)-5-oxo-5,6,7,8-tetrahydro-4H-chromene-3-carbonitrile catalysed by ASS-ZWOM nanocomposite

RT = room temperature, SF = solvent-free, catalyst = ASS-ZWOM nanocomposite

The results indicate that increasing the catalyst amount beyond 0.3 did not further improve the yield, suggesting 0.3 mg of the catalyst is the optimal amount for achieving maximum efficiency. Overall, the use of the ASS-ZWOM nanocomposite as the catalyst in SF conditions proved to be highly effective, offering a rapid and sustainable method for achieving high yields.

### *4.8 Proposed reaction pathway*

The key steps of the reaction mechanism for the formation of the compound (4) in the presence of the ASS-ZWOM nanocomposite catalyst are depicted in **Scheme 2**. The reaction initiates Knoevenagel condensation between malononitrile and aldehyde in the presence of the ASS-ZWOM nanocomposite as the catalyst. This step results in the formation of arylidenemalononitrile (intermediate (I)) through the elimination of water. Next, enolised dimedone (II) undergoes a Michael addition reaction with the intermediate (I), yielding an intermediate product (III). In the final step, the intramolecular cyclization is followed by a rearrangement to produce the desired product (4).

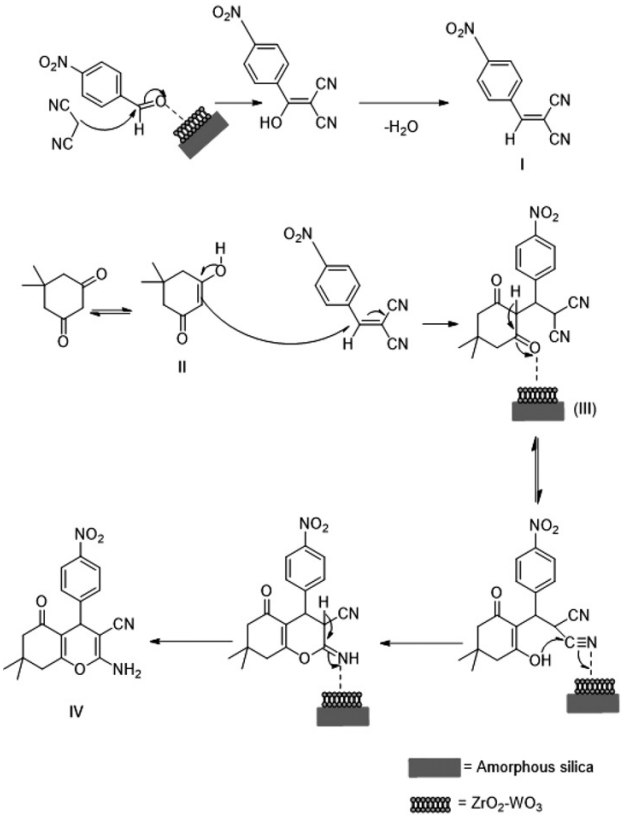


**Scheme 2:** Proposed reaction pathway

## 5 CONCLUSION

Amorphous silica was effectively extracted from coconut coir, a sustainable agro-industrial waste source, utilized for the preparation of an amorphous silica-supported $ZrO_2$-$WO_3$ mesoporous nanocomposite. The characterization of the nanocomposite using FT-IR, XRD, FE-SEM, EDS, Raman spectroscopy, and BET analysis confirmed that the silica was amorphous, while the ASS-ZWOM nanocomposite exhibited a crystalline nature. FE-SEM analysis revealed spherical particles with a porous morphology, silica, and a plate-like structure in the ASS-ZWOM nanocomposite. BET analysis of the ASS-ZWOM nanocomposite showed desirable mesoporous properties, including a moderate surface area and optimized pore-size distribution. The nanocomposite prepared from a cost-effective and eco-friendly source was applied as a heterogeneous catalyst in a three-component reaction. Remarkably, under solvent-free conditions, the ASS-ZWOM nanocomposite demonstrated an excellent catalytic activity, with a shorter reaction time. By integrating agricultural waste into a high-performance nanocomposite, this study bridges the gap between environmental sustainability and industrial demands. The findings made our work both scientifically meaningful and practically useful for advancing sustainable catalytic processes.

## Acknowledgment

We gratefully acknowledge SAPTARSHI at IIT Jammu for granting us access to their high-end characterisation facilities. Our thanks also go to SAIC of Tezpur University in Assam, India, and to the Material Analysis and Research Centre Bengaluru for extending essential analytical support during this work. We are thankful to SAIF, IIT, Roorkee, India, and the Coimbatore Institute of Technology for facilitating additional analyses and characterization essential to this study. This resource and expertise have been invaluable to the success of this research.

## 6 REFERENCES

[1] T. S. Anirudhan, S. Rijith, L. Divya, Preparation and application of a novel functionalized coconut coir pith as a recyclable adsorbent for phosphate removal, Sep Sci Technol, 44 (**2009**), 2774–2796, doi:10.1080/01496390903017899

[2] A. S. Costa, C. M. Paranhos, Mitigation of silica-rich wastes: An alternative to the synthesis of eco-friendly silica-based mesoporous materials, Microporous Mesoporous Mater, 309 (**2020**), 110570, doi:10.1016/j.micromeso.2020.110570

[3] S. N. Azizi, S. Ghasemi, H. Yazdani-Sheldarrei, Synthesis of mesoporous silica (SBA-16) nanoparticles using silica extracted from stem cane ash and its application in electrocatalytic oxidation of methanol, Int J Hydrogen Energy, 38 (**2013**) 36, 16518–16524, doi:10.1016/j.ijhydene.2013.07.086

[4] S. Manimaran, K. Subramanian, R. Tschentscher, A. Pandurangan, Epoxidation of alkene using bi-functional metal oxide supported

SBA-16 catalyst, J Porous Mater, 29 (**2022**), 1025–1037, doi:10.1007/s10934-021-01170-5

[5] D. M. Morales-Paredes, I. Rodríguez-Linz, R. Luque, S. M. Osman, N. Boluda-Botella, et al., Silica-derived materials from agro-industrial waste biomass: Characterization and comparative studies, Environ Res, 231 (**2023**), 116002, doi:10.1016/j.envres.2023.116002

[6] J. Ji, L. Li, L. Quan, B. Tian, P. Zhang, S. Li, The effects of calcination process parameters on RHA reactivity and mortar mechanical properties, Materials, 18 (**2025**) 13, 3129, doi:10.3390/ma18133129

[7] J. G. Santiesteban, J. C. Vartuli, S. Han, R. D. Bastian, C. D. Chang, Influence of the preparative method on the activity of highly acidic $WO_x/ZrO_2$ and the relative acid activity compared with zeolites, J Catal, 168 (**1997**), 431–441, doi:10.1006/jcat.1997.1658

[8] M. Hino, Acid catalysis by solid superacids, Mater Chem Phys, 26 (**1990**) 3, 213–237, doi:10.1016/0254-0584(90)90059-J

[9] H. Wang, Y. Guo, C. Chang, X. Zhu, X. Liu, J. Han, et al., Enhancing tungsten oxide/SBA-15 catalysts for hydrolysis of cellobiose through doping $ZrO_2$, Appl Catal A Gen, 523 (**2016**), 182–192, doi:10.1016/j.apcata.2016.06.006

[10] R. Ramesh, S. Maheswari, J. G. Malecki, $NaN_3$ catalyzed highly convenient access to functionalized 4H-chromenes: A green one-pot approach for diversity amplification, Polycycl Aromat Compd, 39 (**2019**) 8, 609–622, doi:10.1080/10406638.2018.1564678

[11] J. Skommer, D. Wlodkowic, J. Pelkonen, Z. Darzynkiewicz, HA14-1, a small molecule Bcl-2 antagonist, induces apoptosis and modulates action of selected anticancer drugs in follicular lymphoma B cells, Leuk Res, 30 (**2006**) 3, 322–331, doi:10.1016/j.leukres.2005.08.022

[12] E. Abdel, A. Hafez, M. H. Elnagdi, A novel synthesis of benzo[4,5pyrano[2,3-c]quinoline derivatives, Tetrahedron Lett, 26 (**1987**) 12, 1417–1420, doi:10.1016/S0040-4039(00)82357-7

[13] Eastman Kodak Company, New coumarin dyes with rigidized structure for flashlamp-pumped dye lasers, Appl Phys Lett, 13 (**1975**) 1, 3–6, doi:10.1063/1.1654967

[14] M. Balamurugan, S. Saravanan, Producing nanosilica from Sorghum vulgare seed heads, Powder Technol, 224 (**2012**), 345–350, doi:10.1016/j.powtec.2012.03.017

[15] A. Pandurangan, S. Manimaran, Green and recyclable mesoporous silica supported $WO_3$–$ZrO_2$ solid acid catalyst for biodiesel production by transesterification of Ankol seed oil with methanol, Biomass Convers Biorefin, 13 (**2023**), 1543–1554, doi:10.1007/s13399-021-01825-2

[16] S. Sigamani, D. Thirunavukkarasu, M. Rajarajan, Synthesis of $SiO_2$ nanoparticles by sol-gel method and their optical and structural properties, Mater Today Proc, 45 (**2021**), 5956–5961, doi:10.1016/j.matpr.2021.01.237

[17] B. Shokri, M. Abbasi-Firouzjah, S. I. Hosseini, FTIR analysis of silicon dioxide thin film deposited by metal organic-based methods, Surf Coat Technol, 203 (**2009**) 8, 1083–1088, doi:10.1016/j.surfcoat.2008.08.071

[18] S. Narang, S. Rani, P. Aghamkar, S. Kumar, Structural investigations on Nd-doped silica nanocomposites: Effect of sintering temperature and dopant concentration, Mater Sci Semicond Process, 27 (**2014**), 503–513, doi:10.1016/j.mssp.2014.06.030

[19] S. Verma, S. Rani, S. Kumar, Tetragonal zirconia quantum dots in silica matrix prepared by a modified sol–gel protocol, Appl Phys A Mater Sci Process, 124 (**2018**), 1806, doi:10.1007/s00339-018-1806-z

[20] S. Bhaskar, E. W. Awin, K. C. H. Kumar, A. Lale, S. Bernard, R. Kumar, Design of nanoscaled heterojunctions in precursor-derived t-$ZrO_2$/SiOC(N) nanocomposites: Transgressing the boundaries of catalytic activity from UV to visible light, Sci Rep, 10 (**2020**), 1543, doi:10.1038/s41598-019-57394-8

[21] A. E. Goldmane, L. Avotina, M. Romanova, A. Muhin, A. Zaslavskis, G. Kizane, et al., FTIR analysis of oxidized tungsten and tungsten diboride nanolayers, Key Eng Mater, 923 (**2022**), 376–380, doi:10.4028/p-6mtmzn

[22] L. Zhou, Y. Du, Y. Jin, W. Chen, Q. Pan, W. Kai, et al., Grinding-induced solvent-free synthesis of mesoporous zirconia-supported tungsten oxide composite and its superior oxidative desulfurization performance, Fuel, 315 (**2022**), 123181, doi:10.1016/j.fuel.2022.123181

[23] D. Varisli, T. Dogu, G. Dogu, Novel mesoporous nanocomposite $WO_x$-silicate acidic catalysts: Ethylene and diethylether from ethanol, Appl Catal A Gen, 371 (**2009**), 94–101, doi:10.1016/j.apcata.2009.09.033

[24] S. Rajendran, N. W. C. Jusoh, N. Ainirazali, Integrating ZnO with fibrous silica zirconia p–n heterojunction for effective photoredox of hexavalent chromium and congo red, J Water Process Eng, 59 (**2024**), 105050, doi:10.1016/j.jwpe.2024.105050

[25] S. ZrO, M. Catauro, F. Barrino, G. Dal, M. Milazzo, I. Blanco, et al., Structure, drug absorption, bioactive and antibacterial properties of sol–gel derived materials, Ceram Int, 46 (**2020**) 11, 17624–17632, doi:10.1016/j.ceramint.2020.03.167

[26] N. N. Maseko, D. Schneider, S. Wassersleben, D. Enke, S. A. Iwarere, J. Pocock, et al., Production of biogenic silica from different South African agricultural residues through a thermo-chemical treatment method, Mater Today Proc, 38 (**2021**), 64–71, doi:10.1016/j.matpr.2020.05.497

[27] F. Granados-Correa, S. Bulbulian, Influence of textural properties and surface fractal dimensions on the cobalt adsorption behaviour of rice hull ash prepared via solid combustion, J Porous Mater, 28 (**2017**), 641–648, doi:10.1007/s10934-017-0460-6

[28] J. C. Arnaldo, S. Costa, C. M. Paranhos, Systematic evaluation of amorphous silica production from rice husk ashes, J Clean Prod, 196 (**2018**), 674–681, doi:10.1016/j.jclepro.2018.05.028

[29] S. E. Lehman, S. C. Larsen, Zeolite and mesoporous silica nanomaterials: Greener syntheses, environmental applications and biological toxicity, Environ Sci Nano, 1 (**2014**), 200–213, doi:10.1039/C4EN00031E

[30] P. S. Chavan, P. S. Shedge, S. S. Deshmukh, R. R. Bhandalkar, S. H. Sutar, S. H. Mujawar, Electrodeposited tungsten trioxide ($WO_3$) thin films for electrochromic applications, Mater Today Proc, 96 (**2024**), 27–32, doi:10.1016/j.matpr.2024.01.146

[31] M. N. Ashiq, A. Aman, T. Alshahrani, F. Iqbal, A. Razzaq, M. Najam-ul-Haq, et al., Enhanced electrochemical properties of silver-coated zirconia nanoparticles for supercapacitor applications, Nanomaterials, 11 (**2021**) 2, 318, doi:10.3390/nano11020318

[32] K. Song, H. Zhang, Y. Zhang, Y. Tang, K. Tang, Preparation and characterization of $WO_x/ZrO_2$ nanosized catalysts with high $WO_x$ dispersion threshold and acidity, J Catal, 299 (**2013**), 119–128, doi:10.1016/j.jcat.2012.11.011

[33] C. D. Baertsch, S. L. Soled, E. Iglesia, Isotopic and chemical titration of acid sites in tungsten oxide domains supported on zirconia, J Phys Chem B, 105 (**2001**) 7, 1320–1330, doi:10.1021/jp003073d

[34] D. K. Pattanayak, J. Muduli, S. S. Sahu, S. Gouda, S. Meher, T. Dash, S. Rout, P. K. Pattnaik, Production and characterization of amorphous silica nanoparticles from coconut shell and coir, Lett Appl NanoBioScience, 11 (**2021**), 4040–4049, doi:10.33263/LIANBS114.40404049

[35] Q. A. Shabir, A. Pokale, A. Loni, D. R. Johnson, L. T. Canham, R. Fenollosa, M. Tymczenko, et al., Medically biodegradable hydrogenated amorphous silicon microspheres, Silicon, 3 (**2011**) 4, 173–176, doi:10.1007/s12633-011-9097-4

[36] T. H. Bui, T. H. Le, T. K. Pham, H. Q. Pham, Zirconium doped MCM-41 supported $WO_3$ solid acid catalysts for the esterification of oleic acid with methanol, Appl Catal A Gen, 379 (**2010**), 61–68, doi:10.1016/j.apcata.2010.03.001

[37] A. Aziz, S. Shaheen, S. M. A. Nayem, M. N. Shaikh, A. Saeed, I. Akolade, Peat soil-derived silica doped porous graphitic carbon with high yield for high-performance all-solid-state symmetric supercapacitors, Carbon Lett, 32 (**2022**), 427–436, doi:10.1007/s42823-022-00393-3